Received: 10 June 2021 | Revised: 24 December 2021 | Accepted: 31 January 2022

DOI: 10.1002/jev2.12194

RESEARCH ARTICLE

Light-induced high-efficient cellular production of immune functional extracellular vesicles

Shaobo Ruan | **Nina Erwin** | **Mei He**

Department of Pharmaceutics, College of Pharmacy, University of Florida, Gainesville, Florida, USA

Correspondence
Mei He, Department of Pharmaceutics, College of Pharmacy, University of Florida, Gainesville, FL 32610, USA.
Email: MHe@cop.ufl.edu

Funding information
National Institute of General Medical Sciences, Grant/Award Number: 1R35GM133794; National Institute of Food and Agriculture, Grant/Award Number: 2017-67021-26600

Abstract

Extracellular vesicle (EV)-based therapies and vaccines are emerging. However, employment at the scale for population-based dose development is always a huge bottleneck. In order to overcome such a roadblock, we introduce a simple and straightforward approach for promoting cellular production of dendritic cell derived EVs (DEVs) by leveraging phototherapy based light induction. Under the optimization of light wavelengths, intensities, and exposure times, we achieved more than 13-fold enhancement in DEV production rate, while maintaining good integral quality and immune function from produced EVs. The LED light at 365 nm is optimal to reliably trigger enhanced cellular production of EVs no matter cell line types. Our observation and other reported studies support longer near UV wavelength does not impair cell growth. We conducted a series of investigations in terms of size, zeta potential, morphology, immune surface markers and cytokines, biocompatibility, cellular uptake behaviour, and immune-modulation ability on eliciting cellular responses in vitro. We also validated the biodistribution, immunogenicity, and administration safety using light-promoted DEVs in mice models from both male and female genders. Overall data supports that light promoted DEVs are highly immune functional with great biocompatibility for serving as good therapeutic platforms. The in vivo animal study also demonstrated light-promoted DEVs are as well tolerated as native DEVs, with no safety concerns. Taken together, the data supports that light promoted DEVs are in excellent quality, high biocompatibility, in vivo tolerant, and viable for serving as an ideal therapeutic platform in scalable production.

KEYWORDS
extracellular vesicles, high-efficient production, immunomodulation, immunotherapy, light promotion

1 | INTRODUCTION

Dendritic cell (DC) therapy or DC based vaccine development has been emerging in cancer immunotherapy (Ogasawara et al., 2020; Perez & De Palma, 2019; Wang et al., 2020) because DCs are the most potent antigen-presenting cells and are the key initiator of tumour-specific immune responses (Wang et al., 2020). However, due to the unstable characteristics of DCs in vitro and in vivo, current clinical translation and trial development are suffering from inconsistency and low outcomes (Sadeghzadeh et al., 2020). Implementing DC therapy across large populations is costly, difficult to store for long periods, and requires well-defined quality control (Saxena et al., 2018). Compared to DCs, the secreted extracellular vesicles (EVs) possess superior properties to surmount such drawbacks from cell-based immunotherapies, while maintaining immune-modulation and major stimulating molecules, such as the major histocompatibility complex class I (MHC-I) and class II (MHC-II), intercellular adhesion molecule-1

(ICAM-1), integrins, and costimulatory molecules (e.g., CD80, CD86) (Markov et al., 2019; Pitt et al., 2016). Currently, DEV-based phase I and II clinical trials have been conducted with patients in advanced malignancies, which showed feasibility and good safety (Pitt et al., 2016; Pitt et al., 2014; Tian & Li, 2017; Yang et al., 2018). Following the MISEV 2018 guideline, we use a collective term small EVs (sEVs) throughout this paper to cover exosomes as a specific subpopulation of EVs (Théry et al., 2018).

However, producing sufficient amount of EVs for therapy and therapeutic applications has been extremely challenging (Jafari et al., 2020). Conventional cellular culture and secretion is unable to generate quantities that meet clinical dosage needs. Large numbers of cell cultures have to be incubated for days. Unfortunately, current purification of EVs is still in low efficiency. Enhancing the cellular secretion rate for high-efficient production of EVs has been a pressing need (Yamashita et al., 2018). A few attempts have been made to increase the production of EVs via genetic manipulation of biogenesis and recycling pathways in their parent cells, such as the genetically engineered overexpression of activator genes or downregulation of ISGylation involved in EV recycling pathways (Ghossoub et al., 2020; Piffoux et al., 2019; Riquelme et al., 2020; Surman et al., 2019). Such genetic manipulation could induce cellular production which is different than the natural cellular secretion process. Some culture condition engaged methods have been reported to produce more EVs, such as heat shock or radiation treatment, for introducing external stimuli in control of cell proliferation, hypoxia, inflammation, and shear stress (Lamichhane & Jay, 2018; Mcneill et al., 2019; Mitchell et al., 2008). Recently, Lee research group reported a cellular-nanoporation method for the production of large quantities of EVs containing therapeutic mRNAs and targeting peptides through a focal and transient electrical stimulus, which promotes the release of EVs up to 50-fold increase (Yang et al., 2020). However, to date, how the immunogenicity of produced EVs could be changed or posing influences on downstream applications in therapeutic development and drug delivery has not been explored elsewhere, which is critically needed. In order to bridge such knowledge gap, we introduce a simple and novel approach for promoting cellular production of DEVs by leveraging a phototherapy-based LED light, which can significantly increase the EV production by more than 13 folds under our optimized light wavelength, intensity, and exposure time. The optimized light condition at longer near UV 365 nm wavelength does not impair cell growth which is consistent with a reported study of negative impacts on cell gene expression (Wong et al., 2015). Compared to other physical stimulations (e.g., heat shock and electric stimuli), light treatment is relatively simple, straightforward, and can be easily adapted into the cell culture incubators or bioreactors on demand at the manufacturing scale, without the requirement of specific equipment setup.

The immunogenicity and the immunomodulatory function are the central role of EVs in our human body (Robbins & Morelli, 2014), which are highly relevant to their parent cell types, as well as the intra-vesicular and surface molecular compositions. DEVs regulate antigen presentation by carrying membrane and cytoplasmic DC components (Gurunathan et al., 2019; Pitt et al., 2016; Utsugi-Kobukai et al., 2003), including MHC-I and MHC-II, ICAM-1, integrins, and T cell costimulatory molecules (e.g., CD80, and CD86), which are critical for the activation of adaptive immune responses (Chaput et al., 2006; Morelli et al., 2004; Munich et al., 2012). Accumulating evidence suggested that DEVs could modulate immune response either directly by exposing MHC-antigen complexes and costimulatory molecules to T cells, or indirectly by conveying antigens to surrounding DCs (Fernández-Delgado et al., 2020). In order to assess the influence of light induced production on such EV immune functions, we investigated three major immune markers from produced EVs, including MHC-I, MHC-II, and CD86, which did not show significant changes compared to the control group without light treatment from both immature DCs and mature DCs. The immunomodulation function, immunogenicity, oxidative stress levels, and biocompatibility of light-promoted EVs from both their parent immature (imDCs) or mature DCs (mDCs) are also comparable to naturally produced EVs both in vitro and in vivo. The in vivo animal study on biodistribution of light-promoted DEVs showed very high similarity (> 98%) with naturally derived DEVs. The immune profiling of single-cell suspended immune cells from the mice spleens and lymph nodes exhibits no difference between light-promoted DEVs and naturally derived DEVs, and both are well tolerated. The immunity elicitation is highly comparable with no safety concerns. In contrast, the light-promoted DEVs have significantly enhanced production rates. We anticipate this simple method could serve as an effective strategy for high-speed production of EVs with good immunogenicity as a drug delivery vehicle or therapeutic agent, which could solve the bottleneck challenge in the clinical translation of developing a DEVs based therapy.

2 | MATERIALS AND METHODS

2.1 | Cell culture and preparation

Antigen presenting JAWS II cells were cultured in alpha-MEM (minimum essential medium α) medium (Gibco, USA) containing 20% fetal bovine serum (FBS, Gibco, USA), 1% penicillin-streptomycin (Corning, Arizona, USA) and 5 ng/ml recombinant mouse granulocyte macrophage colony-stimulating factor (GM-CSF) (R&D Systems, USA). IC-21 macrophages were cultured in RPMI-1640 medium (ATCC, USA) containing 10% FBS and 1% penicillin-streptomycin. Human umbilical vein endothelial cells (HUVEC) were cultured in F-12K medium (gibco, USA) containing 10% FBS, 1% penicillin-streptomycin, 0.1 mg/ml heparin (Sigma, USA) and 30 μg/ml endothelial cell growth supplement (ECGS, Fisher Scientific, USA). Subcultures were maintained

in humidified incubator with 5% CO_2 supply at 37 °C and all experiments were performed during the logarithmic phase of cell growth.

2.2 | Culture and maturation of mouse bone marrow DC cell line JAWS II

Immature JAWS II cells were passaged into T-25 (25 cm^2) flasks and allowed to grow 2 days (approximately 40% confluency). Afterwards, LPS (LPS from *E.coli* O111:B4 strain) predissolved in endotoxin-free water (1 mg/ml) was introduced into the culture medium at a final concentration of 100 ng/ml for another 2 days of culture to induce JAWS II cell maturation. For UV condition screening, immature JAWS II cells were passaged into T-25 (25 cm^2) flasks and allowed to grow for 4 days (approximately 80% confluency). Then, cell cultures were exposed under near-UV LED light (OmniCure AC450/P-365UV), at different wavelengths, time durations (5, 10, 15, 20 and 30 min) and light intensities (1.6, 2.4, 3.2 and 4.0 W/cm^2) at fixed distance of 10 cm, which converted to the actual exposure intensities on cells at 0.064, 0.096, 0.128 and 0.16 W/cm^2. The OmniCure AC450/P air-cooled UV LED light has a flat light output window large enough to cover the entire cell culture flask with uniform LED light exposure. By experimental optimization, 0.096 W/cm^2 for 30 min of light treatment at a fixed distance of 10 cm was selected for cell treatments, as discussed in the result section.

2.3 | EV purification and characterization

JAWS II cells were passaged into T-25 (25 cm^2) flasks and treated with different conditions (near-UV LED light treatment on both imDCs and mDCs) as described above. Immature JAWS II cells without any treatment were set as the control group. The culture medium was then discarded and replaced with fresh medium containing EV-depleted FBS (Gibco, USA) for 48 h. Then, cell culture supernatants from differently conditioned JAWS II cells were collected. JAWS II cells-derived EVs were isolated from the supernatant by sequential ultracentrifugation process, as previously reported (Li et al., 2017; Thery et al., 2006). In brief, cells were removed from the supernatant by centrifugation at 300 g for 10 min followed by removing cell debris at 2000 g for 30 min. To remove any possible apoptotic bodies and large cell debris, the supernatants were then centrifuged at 10,000 g for 30 min. Finally, culture medium was transferred to ultracentrifuge tubes (Thermo Scientific, USA) and small EVs were collected by ultracentrifugation at 100,000 g for 70 min (Sorvall MTX150 Micro-Ultracentrifuge, USA). Then, small EVs were further washed in 10 ml PBS and pelleted again by ultracentrifugation (100,000 g for 70 min). Purified small EVs were resuspended in 500 μl ice-cold PBS for further study or storage in -80 °C.

The size and particle number of isolated small EVs were analysed by nanoparticle tracking analysis (NTA) using the NanoSight LM10 instrument (Malvern Instruments, UK) equipped with a blue laser (405 nm). Briefly, 25 μl of the final pellet suspension was diluted at 1:20 for EVs derived from mDCs or imDCs and 1:100 for EVs derived from light promoted DEVs. A solution of 300 μl was injected into the sample chamber of LM10 unit and five videos of 30 s trajectory monitoring were recorded for each sample. Data analysis was performed with NTA 3.4 software (NanoSight). Software settings for capture and analysis were showed as followed: camera level = 16, screen gain = 1, detection threshold = 5. The zeta potential of isolated small EVs was determined by dynamic laser scattering (ZS90 Zetasizer, Malvern Instruments). The morphology of isolated small EVs was verified by transmission electron microscopy (TEM, FEI Spirit TEM 120 kV) imaging following the protocol described previously (Lázaro-Ibáñez et al., 2014). Briefly, ultrathin copper grids coated with 400 mesh carbon film (FCF400-Cu-UB, Electron Microscopy Science, USA) was used with glow discharge treatment for 1 min before use. Then, 5 μl EV samples were individually added onto the glow-discharged grids and were quiescent for 10 min at room temperature. The grids were washed with distilled water one time, then negatively stained with filtered 2% aqueous uranyl acetate for 2 min, and dried at room temperature before observation. The TEM imaging power was set at 120 kV by FEI Spirit G2 with a digital camera (Soft Image System, Morada and Gatan Orius SC 1000B CCD-camera).

2.4 | NanoView microarray for characterization of EV surface markers

Culture medium was collected and centrifuged at 300 g×10 min, 2000 g×30 min, and 10000 g×30 min sequentially to remove cell debris. Per standard protocols provided by NanoView Biosciences (Brighton, MA, USA), processed culture media was diluted appropriately using the EV binding buffer (solution A, pH7.4), then 35 μl of diluted sample was dropped on microarray chips for incubation overnight. Three chip spots were each precoated with capture antibodies CD81 (clone Eat-2, mouse, Biolegend), CD9 (clone MZ3, mouse, Biolegend), and negative controls HIgG (clone HTK888, mouse, Biolegend) and RIgG (clone RTK2758, Biolegend). Microarray chips were washed four times with solution A at 150 rpm/min, for 3 min each time. After washing, 300 μl blocking solution was incubated with each chip for 1 h at room temperature and protected from light, which contains three detection antibodies including 0.6 μl Alexa Fluor@647-conjugated CD63 (clone NVG-2, Biolegend), 2 μl Alexa

Fluor@488-conjugated CD86 (clone GL-1, Biolegend), and 2.5 μl PE-conjugated MHC class I (mouse, clone AF6-88.5.5.3, Invitrogen) or MHC class II (mouse, clone M5/114.15.2, Invitrogen). Following, microarray chips were washed again with solution A, solution B, and distilled water, sequentially. Then chips were air dried for imaging by ExoView R100 (NanoView Biosciences), equipped with a 40x objective lens (Olympus, Japan). Data was analysed and quantified using off-line ExoViewer3 EAP_v3 software.

2.5 | In vitro cellular uptake analysis

EVs with a total number of 1×10^{10} were diluted with diluent C to a final volume of 1 ml, per instruction of PKH-26 labelling kit (Sigma, USA). 6 μl PKH-26 dye solution was added and mixed gently, followed by incubation at room temperature for 5 min (protected from light). The labelling was quenched by adding 2 ml cold 10% BSA in PBS, bringing the volume up to 8 ml. Afterwards, 2 ml 0.971 M sucrose solution was added by pipetting slowly and carefully into the bottom of the ultracentrifuge tubes, maintaining the EV-PKH26 solution on the top of the sucrose cushion. The solution was then centrifuged at 100,000 g for 90 min at 4°C. The entire solution, including the sucrose layer, was aspirated carefully, retaining the EV pellet for resuspension in 10 ml cold PBS, followed by centrifuge filtration to remove free dyes using Amicon ultra centrifugal filter (10 kDa MWCF, Millipore Sigma, Missouri, USA) at 3000 g for 40 min at 4°C.

For flow cytometry analysis of JAWS II cell uptake, JAWS II cells were seeded into 24-well plates at a density of 5×10^4 per well and allowed to grow for two more days (approximately 80% confluency). Then, the culture medium was discarded and replaced with fresh culture medium containing PKH-26 labelled EVs (1×10^9 particles per cell). After 1, 2, 4, and 24 h incubation, cells were digested, harvested, and washed with PBS twice. Finally, cells were resuspended in 500 μl PBS for flow cytometry analysis. The fluorescence intensity was detected at PE channel using Fortessa multicolour flow cytometer (BD Biosciences, USA). For IC-21 uptake, IC-21 cells were seeded into 12-well plates at a density of 1×10^5 per well and allowed to grow for three more days (approximately 80% confluency). The following incubation, cell harvest, resuspension, and analysis were same as the procedures described above.

For confocal microscopic imaging, JAWS II cells were seeded into 6-well plates preplaced with 400 mm^2 coverslip at a density of about 2×10^5 per well and allowed to grow for 2 days. The medium was then removed and replaced with fresh FBS-free medium containing PKH-67-labeled EV samples at a concentration of 1×10^9 for another 1, 2 and 4 h incubation. 30 min before the end of incubation, lysotracker-red (DND-99, Invitrogen, USA) was introduced into the medium at a final concentration of 100 nM. Then, cells were washed twice, fixed with 4% paraformaldehyde for 20 min at room temperature, and counterstained with 4′,6-diamidino-2-phenylindole (DAPI, 0.5 μg/ml) for another 5 min. The coverslips were transferred onto glass microscope slides and were applied a drop of antifade mounting media (Thermo Fisher, USA). Fluorescence was captured using Nikon Ti2 fluorescence microscope (Japan).

2.6 | MTT assay

To test the cell viability after 365 nm light treatment, different light intensities (0.064, 0.096, 0.128 and 0.16 W/cm^2) and time durations (5, 10, 15, 20 and 30 min) were applied to both mature and immature JAWS II DC cells. Afterwards, the culture medium was replaced with fresh complete culture medium and allowed to grow for another 2 days. Then, cells were harvested, centrifuged, and seeded into 96-well plates at a density of ~ 5000 cells per well, followed by adding 10 μl 3-(4,5-dimethylthiazol-2-yl)-2,5-diphenyltetrazolium bromide (MTT, 5 mg/ml). The immature JAWS II DC cells without light treatment were used as the control group. Cells were processed following the MTT assay protocols per vendor's instruction (Cell Proliferation Assay Kit, Thermo Fisher) and the absorbance was measured at 570 nm. To test the biocompatibility of secreted DC EVs, JAWS II DC cells were seeded into 96-well plates at a density of ~ 2000 cells per well and allowed to grow for 2 days. The medium was then removed and replaced with fresh medium containing different concentrations of DC EVs (1.25×10^8, 2.5×10^8, 5×10^8, 1×10^9 particles) for incubation at 24, 48, and 72 h. 10 μl of the MTT (5 mg/ml) solution was added into the culture medium at a final concentration of 10% and further incubated for another 4 h. After incubation, the culture medium was removed and then added with 150 μl dimethyl sulfoxide per well. The plates were incubated at 150 rpm/min at 37 °C for 15 min and the absorbance was measured at 570 nm using a microplate reader (Biotek, USA). The immature JAWS II DC cells without incubation with DC EVs were used as the control group.

2.7 | Immune-stimulatory functional assessment

JAWS II cells were seeded into 12-well plates at a density of ~1×10^5 per well and allowed to grow for 2 days. The medium was then removed and replaced with fresh FBS-free medium containing EV samples at a concentration of 1×10^9 for incubation at 24, 48

and 72 h. Afterward, cells were harvested and washed with PBS twice, then suspended in 100 μl PBS for flow cytometry analysis of immune-modulatory markers including MHC-I, MHC-II, and CD86. For single-color staining, cells suspension (1×10^6 cells) in 100 μl of ice-cold flow cytometry buffer (PBS, 1% BSA, 0.1% sodium azide) were stained with PE-conjugated MHC-I (clone AF6-88.5.5.3, Invitrogen, 0.25 μg/test), MHC-II (clone M5/114.15.2, Invitrogen, 0.25 μg/test), and CD86 (clone GL-1, Invitrogen, 0.25 μg/test) for 1 h at 4 °C in the dark. After staining, cells were washed three times by centrifugation at 400 g for 3 min and resuspended in 500 μl of ice-cold flow cytometry buffer. In parallel, cells stained with PE-conjugated isotype control antibodies were set as the negative control. The fluorescence intensity was detected at PE channel using Fortessa multicolour flow cytometer (BD Biosciences, USA). For double-colour staining, the cell suspension (1×10^6 cells) in 100 μl of ice-cold flow cytometry buffer (PBS, 1% BSA, 0.1% sodium azide) was double-stained with Alexa Fluor 488-conjugated CD86 (clone GL-1, Biolegend, 0.25 μg/test) and PE-conjugated MHC class I (0.25 μg/test) or MHC class II (0.25 μg/test) for 1 h at 4 °C in the dark. The fluorescence intensity was detected at FITC and PE channels with appropriate compensation using Fortessa multicolour flow cytometer (BD Biosciences, USA).

To determine TNF-α secretion into culture medium, the supernatant was collected after EV isolation. The concentration of TNF-α in the supernatant was detected by TNF-α ELISA Kit (mouse, Invitrogen, USA) according to manufacturing protocols. In brief, 50 μl/well of the supernatant under different conditions was added into the microwell strip precoated with antimouse TNF-α,followed by 50 μl/well of biotin-conjugated antibody for 2 h incubation at room temperature with shaking (75 rpm/min). ~100 μl/well of diluted streptavidin-HRP was incubated for 1 h to develope chemiluminescent detection with ~100 μl/well of tetramethylbenzidine (TMB) substrate for another 15 min incubation at room temperature. ~100 μl/well of stop solution was applied and then read at 450 nm using a microplate reader. To determine TNF-α in the EVs, 100 μl of EVs were first lysed with 50 μl of radio-immune precipitation assay (RIPA) buffer (Thermo Fisher, USA) containing 1% protease inhibitor cocktail (Thermo fisher, USA). The concentration of TNF-α carried by EVs was then detected according to the protocol described above.

2.8 | Oxidative stress analysis

To determine whether cell-stress pathways in cells are activated by light treatment, immature and mature DC cells were treated with 365 nm UV light (0.096 W/cm2, 30 min), and then seeded into 96-well plates at a density of ~ 2000 cells per well. Cells were allowed to grow 1, 48, and 96 h post light treatment. Then, 5 μM CellROX Deep Red Reagent in dimethyl sulfoxide was added to each well and the plates were incubated at 37 °C for 30 min. The presence of reactive oxygen species was measured through fluorescence intensity readings at an excitation of 630 nm and emission of 675 nm using a microplate reader (Biotek, USA). Untreated mature and immature cells were set as a control, along with 800 μM hydrogen peroxide treated cells as the positive control.

To test the effect of light promoted EVs on recipient cells, EVs were collected after two days of culture in fresh medium from imDC and mDC cells with light treatment at 0.096 W/cm2 for 30 min. Then, imDC cells were seeded into 96-well plates at a density of ~ 2000 cells per well with the different DEV samples at variable concentrations (0, 2.3×10^6, 5.5×10^7 particles) for incubation at 24, 48, and 72 h. Then, 5 μM CellROX Deep Red Reagent in dimethyl sulfoxide was added to each well and the plates were incubated at 37 °C for 30 min. After incubation, the presence of reactive oxygen species in the recipient cells was measured through fluorescence intensity readings at an excitation of 630 nm and emission of 675 nm using a microplate reader (Biotek, USA). The imDC EVs and mDC EVs were set as the control groups. The 800 μM hydrogen peroxide treated imDC cells were set as the positive control group.

2.9 | In vivo biodistribution study

To perform in vivo biodistribution study, EVs were first labelled with a near-infrared lipophilic carbocyanine dye DiR (Invitrogen, USA). Briefly, 5 μl of DiR, at a concentration of 1 mg/ml in ethanol, was mixed with 5×10^{10} EVs in 1 ml PBS and incubated at room temperature for 20 min. Subsequent spin column purification was performed to remove ethanol and unincorporated DiR according to PKH-67 labelling protocol described above. Both male ($n = 4$) and female ($n = 4$) C57BL/6 mice were intravenously injected with freshly prepared DiR-labelled EV samples through the tail at a dose of 1×10^{10} EVs (~0.15 ml) per mouse. The in vivo biodistribution of these DiR-labelled EVs in live mice at 2, 6, 24, 48, and 72 h was evaluated using IVIS Lumina II optical imaging system (Xenogen, Caliper Life Science, USA). Before imaging, mice were preanaesthetized using 2–4% isoflurane in 100% oxygen. Subsequently, the mice were euthanized and major organs (heart, liver, lung, kidney, spleen, and lymph nodes) were harvested at the last time interval of 72 h for ex vivo imaging. Imaging conditions: fluorescence imaging with filter sets was used to perform optical studies. The scanning parameters include: excitation = 730 nm, emission = 780 nm, field of view = 13.5 cm, and fluency rate = 2 mW cm^{-2}. The camera was set to a maximum gain, with a binning factor of 4, and a luminescent exposure time of 4 s. The data was analysed with the IVIS software (Living Image Software for IVIS). All procedures were approved by the IACUC committee of the University of Florida and followed the guidelines established by NIH.

2.10 | Evaluation of in vivo immunogenicity

Male and female C57BL/6 mice were intravenously injected with different freshly prepared EV samples through the tail at an equivalent dose of 1×10^{10} EVs per mouse, respectively. 72 h postinjection, spleen and lymph nodes (LNs) were isolated and prepared into single-cell suspensions. Briefly, spleens and LNs were grinded and homogenized in fresh RPMI-1640 medium, then filtered with a 70 μm cell strainer (Fisher Scientific). Before homogenization in RPMI-1640 medium, the grinded LNs were preincubated with 1 mg/ml of Collagenase IV (Stemcell Technologies, USA) for 30 min under the condition of 37 °C and 75 rpm/min. The resulting cells were washed with PBS and lysed by red blood cell lysis buffer (Thermo Fisher, USA). To analyse DCs maturation, splenocytes and lymphocytes were double-stained with FITC-anti-CD86 antibody and PE-anti-CD11c antibody, PE-anti-MHC-I antibody, as well as PE-anti-MHC-II antibody. All samples were analysed using Fortessa multicolour flow cytometer (BD Biosciences, USA) at FITC and PE channels with appropriate compensation and 50,000 events were counted for each sample. In addition, peripheral blood was collected simultaneously from mice to isolate serum for TNF-α ELISA analysis.

2.11 | Statistical analyses

Multiple comparisons between different groups were analysed by one-way AVONA. A comparison between the experimental group and control group was analysed by the paired Student's t-test. $p < 0.0332$, 0.0021, 0.0002, and 0.0001 were considered a statistically significant difference and remarked with *, **, *** and ****, respectively.

3 | RESULTS AND DISCUSSION

3.1 | Near-UV LED light promotes high-efficient cellular production of EVs

The influences of LED light from different wavelengths (365 nm, 405 nm, and 488 nm) and intensities on the secretion dynamics of EVs have been investigated using JAWS II cell, a mouse bone marrow DC cell line. We observed that near UV LED at 365 nm can promote high-efficient EV production from cultured cells compared to that at 405 nm or 488 nm (Figure S1). The efficiency of LED light at 365 nm to trigger EVs production was found to be highly dependent on light intensity and exposure time. Higher light intensity and longer exposure times, resulted in more production of EVs (Figures S2 and S3). After testing several light conditions, we found that a threshold of light exposure with intensity at 0.096 W/cm^2 for 30 min was able to efficiently turn on the cellular machinery for highly enhanced production of EVs, as compared with their corresponding cells without light treatment. A similar observation on IC-21 cells (a mouse macrophage cell line) and HUVEC cells supports that near UV LED at 365 nm is optimal to reliably trigger enhanced cellular production of EVs (Figure S4). We chose JAWS II mainly for the investigation because it is a professional antigen presenting cell line essential in immunity regulation and is well documented as the most stable DC cell line for cross reference. At such optimized light exposure conditions, the average ability of cellular secretion of EVs was significantly increased, regardless of their mature or immature status. As expected, about 13.3-fold or 5.1-fold enhancement of EV secretion from both light-induced imDCs (UV-imDEVs) or mDCs (UV-mDEVs) were observed, compared to EVs from imDCs (imDEVs) or mDCs (mDEVs) without light exposure (Figure 1a). The light promoted EVs were still maintaining similar size (Figure 1b), zeta potential (Figure 1c), and morphology (Figure 1e) compared to their corresponding control groups without light treatment. Additionally, we investigated TNF-α level from secreted DEVs, as TNF-α is an essential proinflammatory cytokine for immunity regulation. We did not observe noticeable changes in TNF-α levels from light produced imDEVs or mDEVs compared to their corresponding control groups, which indicated that consistent immune modulator function is retained using our optimized light treatment, while the EV production rate is significantly enhanced (Figure 1d).

Although light wavelengths around or below 310 nm has been reported to be harmful for cell viability (Masuma et al., 2013), and 250–270 nm UV light could induce gene damage and cell apoptosis (Gao et al., 2013; Gary & Rochette, 2020), the influence of longer wavelengths at 365 nm light on cell growth remains to be investigated. We study the cell viability of imDCs under the influence of different exposure times and intensities of 365 nm LED light as shown in Figure S5a. 2 days after light treatment, the majority of cells could maintain good cell viability (> 80%) under light intensity below 0.128 W/cm^2. Under our optimized light conditions (0.096 W/cm^2-30 min), we further confirmed the cell viability of either imDCs or mDCs, which showed a slight decrease compared to corresponding control cells without light treatment (Figure S5b). We observed that light treated DC cells require two more days to reach 90–100% confluency compared to their native cells without light treatment which require 4 days to reach confluency for subculture (Figure S5c). At the confluency status, the cells have similar growth capacity regardless of the influence of light treatment (Figure S5d). The data suggested that optimized near UV 365 nm light (0.096 W/cm^2–30 min) may slightly influence cell growth but could recover to normal status in 2 days. In order to further assess whether light treatment could activate the cell-stress pathway, we tested the production and accumulation of reactive oxygen species (ROS) in cells under our optimized light conditions (0.096 W/cm^2–30 min) as shown in Figure 2(a). The light treatment groups did not show significant

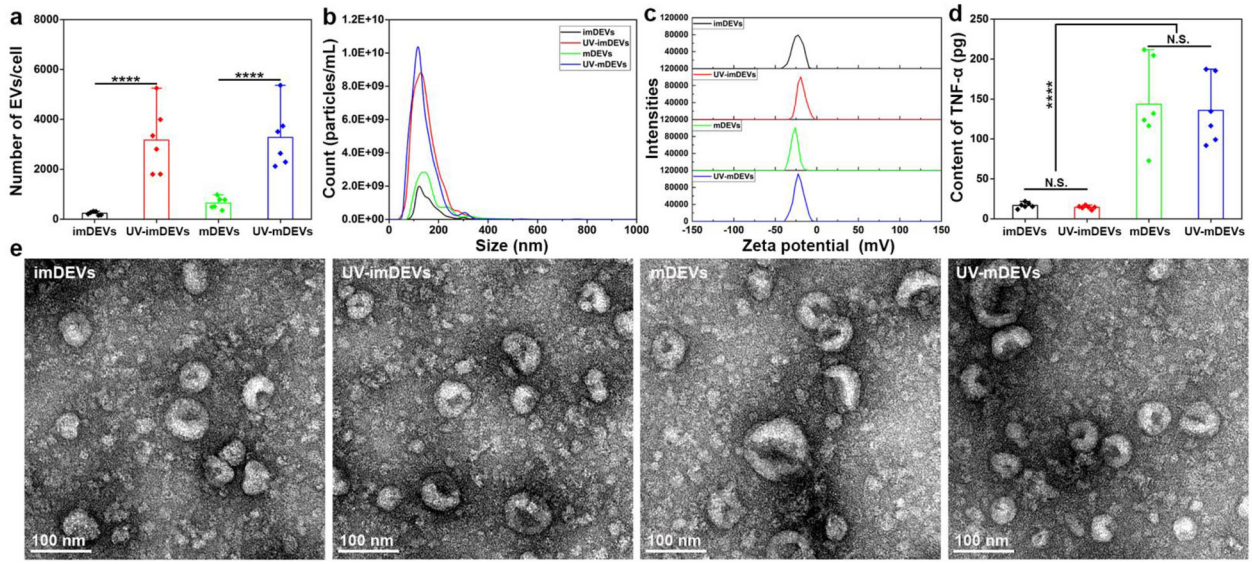

FIGURE 1 Characterization of light-promoted cellular production of EVs. (a) Average cellular secretion rate for EV production from both imDCs and mDCs after light treatment ($n = 6$, each point corresponding to a separate experiment done on a different day). $^{****}p < 0.0001$. (b) NTA analysis of size distribution of light-promoted EVs, indicating the consistent size range compared to the control group EVs without light treatment (NTA plot is from the average of 5 independent measurements). (c) Zeta potential profiles from light-promoted EVs which is consistent with their control group without light treatment. (d) The TNF-α level carried by light-promoted EVs which is consistent with the control group of native EVs ($n = 6$). (e) TEM images showing the morphology of light-promoted EVs secreted from both imDCs and mDCs, which is consistent with the control group of native EVs

differences compared to the control group without light treatment in terms of ROS level, along the time course of 1, 48, and 96 h post light treatment. In contrast, the positive control group of DCs treated with H_2O_2 displayed a significantly enhanced ROS level, and the ROS level gradually reduced along time until 96 h (Figure 2a). We also investigated whether the light promoted DC EVs can induce cellular oxidative stress on recipient cells. We harvested EVs after 2 days of culture from light treated DCs, compared with EVs derived from DCs without light treatment as the control group. By applying different concentrations of DEVs ($0, 2.5\times10^6, 5.5\times10^7$ particles) for dosing recipient imDCs, we monitored the ROS level after 24 , 48, and 72 h, and did not observe noticeable differences from light-promoted DEVs compared with control groups. It has been reported that low-dose, long-wave UV light does not affect gene expression from human mesenchymal stem cells (Wong et al., 2015). Our observation is in line with the reported study. The parent DCs can be passaged for continuous usage.

In order to maintain sustainable, high-efficient EV production ability from cell cultures, we also investigated the parent cell immune function after light treatment. Serving as the crucial antigen presenting cell, DCs, particularly mDCs, express surface markers MHC-I, MHC-II, and CD86 for regulating immune responses and activating T cells. We studied those essential surface marker expression levels via flow cytometry and did not observe a noticeable influence of light treatment on imDCs (Figure 3a and b). For the mDCs group, much higher expression levels (~7-9 fold) of MHC-I, MHC-II, and CD86 was observed compared to the imDCs as expected. However, the light treatment led to reduced marker expressions by nearly half (Figure 3a and b). In our cytokine study, parent cell TNF-α levels were slightly reduced from both imDCs and mDCs (Figure 3c) after light treatment, but the TNF- α level carried by their correspondingly secreted EVs remained the same (Figure 1d). We suspected such reduction of surface marker expressions (MHC-I, MHC-II, and CD86) from mDCs (Figure 1b) could be attributed to substantially increased output transport via EVs. Therefore, for further clarification, we investigated immune marker expression levels from secreted EVs in the next step.

3.2 | Assess the immune marker expression from light promoted DEVs

In order to further characterize the immune activity of light-promoted DEVs, we employed a single-EV microarray imaging technology from NanoView to directly determine whether light promoted DEVs are significantly immune potent with expression of functional markers. The specific antibody capture on each NanoView chip spot allows the antibody capture-based immobilization of EV samples for further immune-probing with up to three fluorescently labelled antibodies (here used CD63, MHC-I/-II, and CD86 antibodies) (Figure 4a). Fluorescent images of CD81 and CD9 capture spots displayed each single EV clearly with either individual or colocalization of antibody probing (CD63 in red, MHC-I/II in green, CD86 in blue) (Figure 4b, S6). The isotype spots (HIgG or RIgG) were used as the background and nonspecific control (Figures S7 and S8), which showed

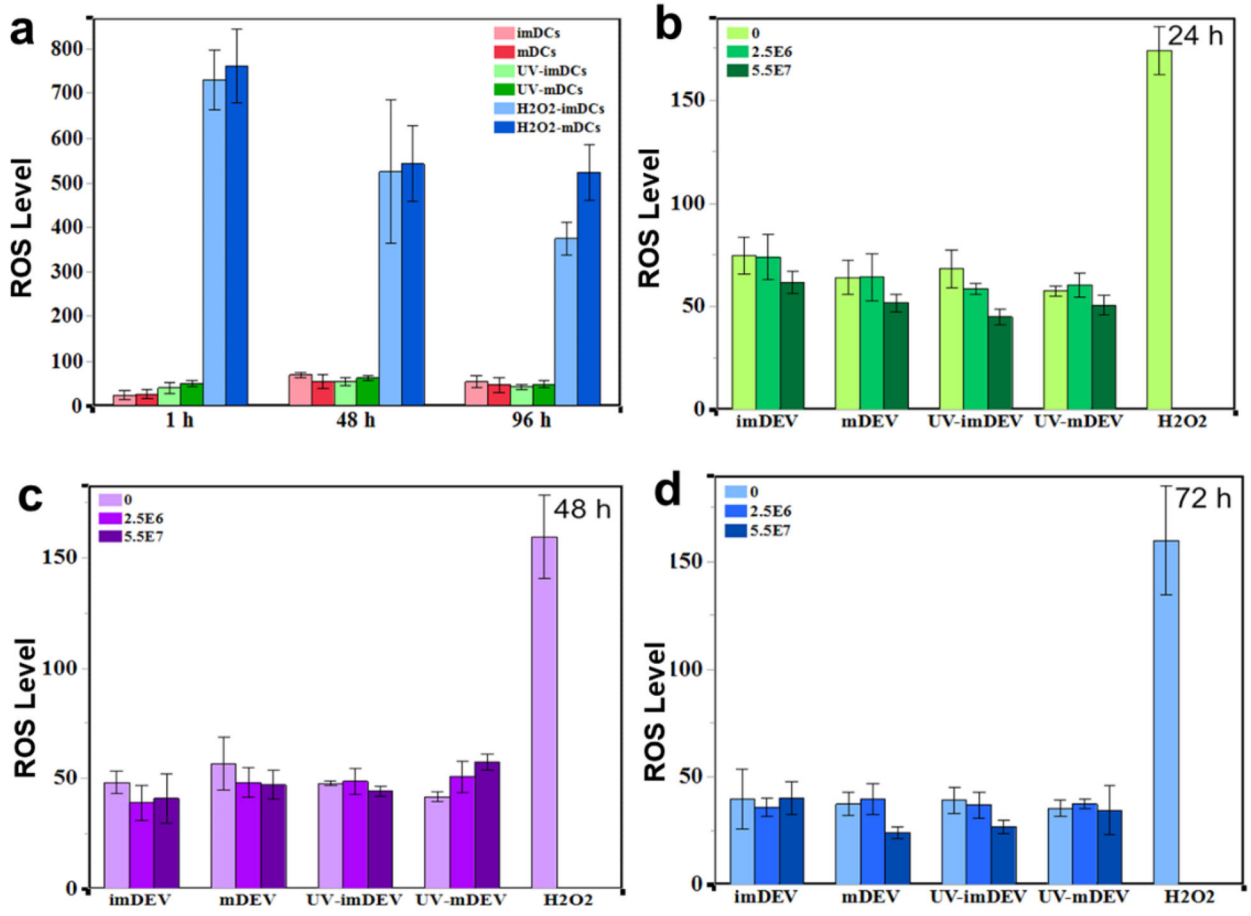

FIGURE 2 (a) Characterization of cellular oxidative stress levels from light treated DCs monitored 1 h post light treatment till 96 h. The DCs without light treatment serve as the negative control group, and the H_2O_2 treated DCs serve as the positive control group. All values are presented as means ± SD ($n = 4$). (b) Characterization of cellular oxidative stress levels from imDCs after uptaking light promoted DC EVs at different doses and monitored at 24 h (b), 48 h (c), and 72 h (d). The EVs derived from DCs without light treatment serve as the negative control group, and the H_2O_2 treated DCs serve as the positive control group. All values are presented as means ± SD ($n = 4$)

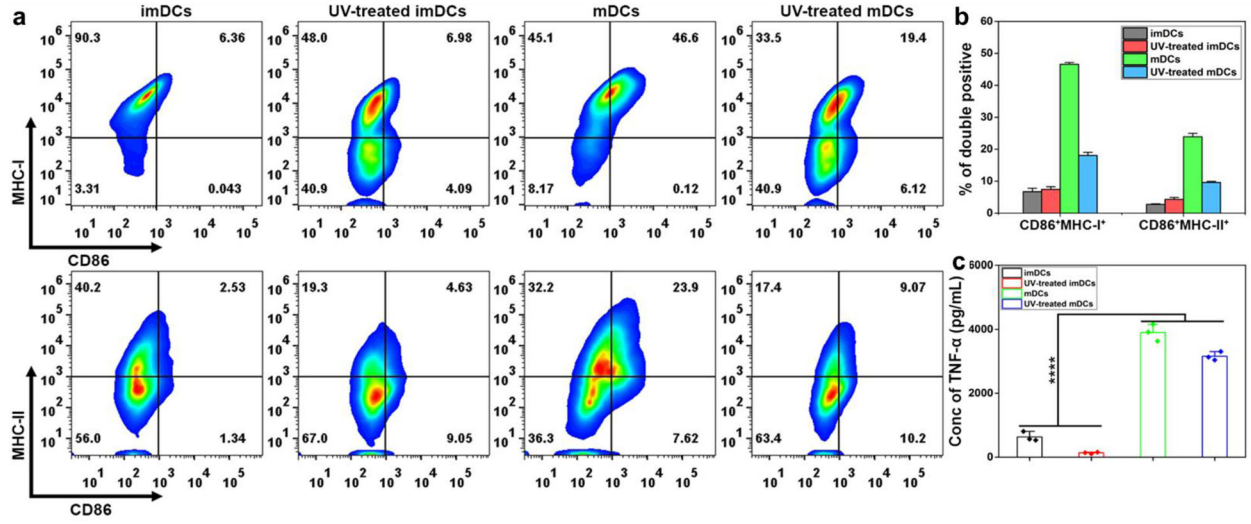

FIGURE 3 (a) Representative flow cytometry analysis of MHC-I, MHC-II, and CD86 marker expression levels from immature and mature DCs with or without light treatment. Cells were immunostained with AF488-conjugated CD86 and PE-conjugated MHC class I/II. (b) Quantitative analysis of marker expression levels from immature and mature DCs with or without light treatment ($n = 3$). (c) The TNF-α level in the culture medium secreted by both immature and mature DCs with or without light treatment. All values are presented as means ± SD ($n = 3$). ****$p < 0.0001$

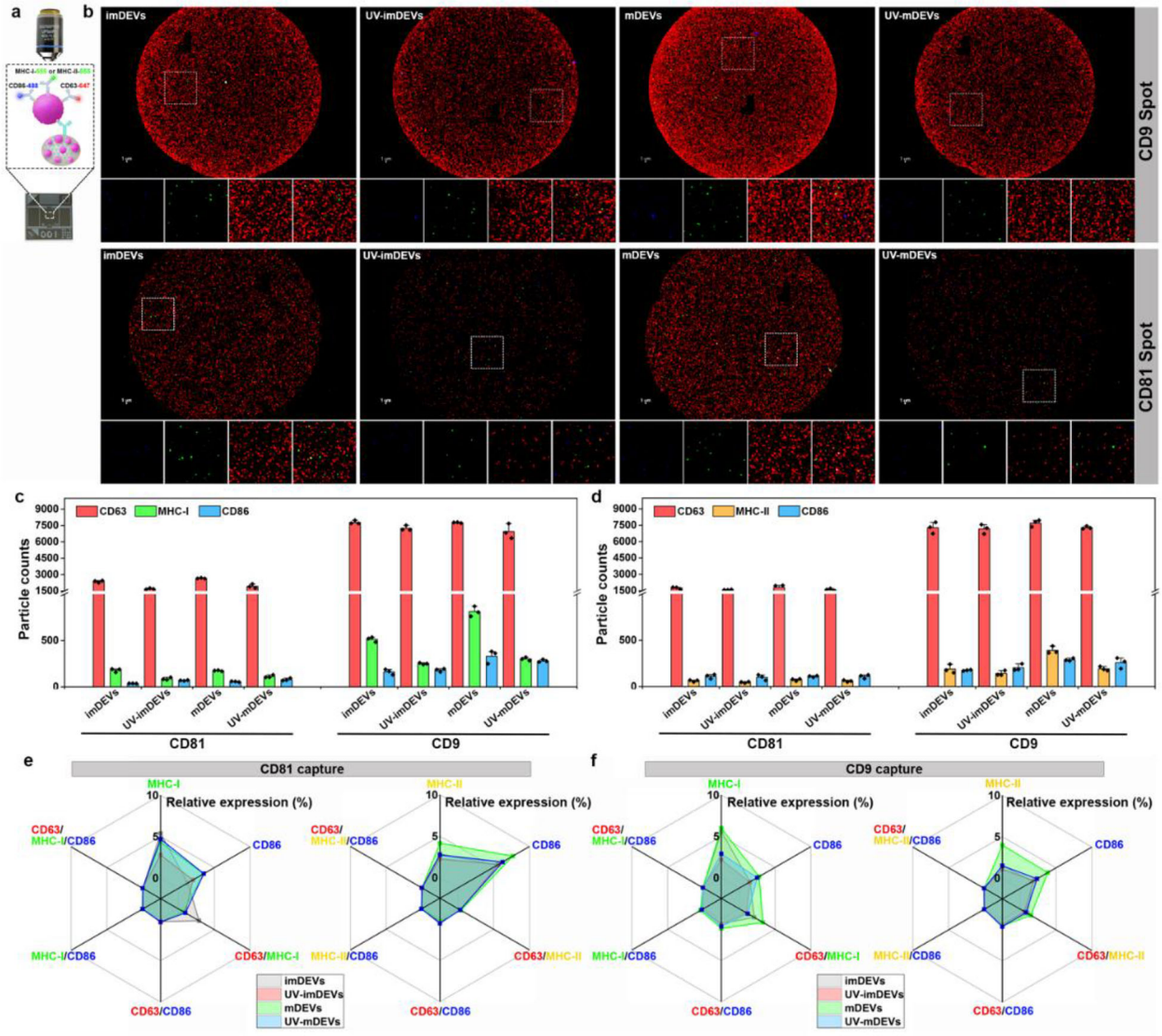

FIGURE 4 Evaluation of the immune marker expression from light promoted DEVs using NanoView single-EV microarray. (a) Schematic diagram of sensitive multimarker detection from EVs captured on microarray chip spot. (b) Representative fluorescent microarray imaging of $CD63^+$ (red), $MHC\text{-}I^+$ (green), $CD86^+$ (blue) DEVs on CD9 (upper) and CD81 (lower) capture spots. Bottom image frames are enlarged views of captured EVs under each fluorescent channel as well as the overlay. (c) Particle counts of captured $CD63^+$, $MHC\text{-}I^+$, and $CD86^+$ DEVs from different EV sample conditions on both CD81 and CD9 capture spots ($n = 3$). (d) Particle counts of captured $CD63^+$, $MHC\text{-}II^+$, and $CD86^+$ EVs from different EV sample conditions on both CD81 and CD9 capture spots ($n = 3$). (e) Radar chart analysis of the relative coexpression levels of multimarkers in various combinations from different EV sample conditions on both CD81 and CD9 capture spots (f)

negligible EVs capture in either total counts or individual marker counts. We observed that the total EV counts from CD9 antibody capture were always about 4-fold higher than that from CD81 antibody capture, regardless of the measurement settings, which may indicate that majority populations of DEVs possess the CD9 expression, but not CD81 expression (Figure 4c and d). Thus, probing immune functional surface markers MHC-I, MHC-II, and CD86 from CD9 captured EVs could better represent the immune potency from the total population of light promoted DEVs.

CD63 is a common structural and functional protein during EV biogenesis, which makes $CD63^+$ EV counts much higher than that from $MHC\text{-}I^+$ and $CD86^+$ counts. On the other hand, CD63 can serve as the internal EV reference marker to assess total captured EVs, which exhibits comparable abundance between all samples and chip spots, indicating consistent and reproducible measurements (Figure 4c and d). With CD63 as the internal reference, we conducted two parallel measurements to assess the expression levels of both MHC-I and MHC-II with CD86 under the influence of our light-based EV production conditions in Figure 4(c) and (d). The relative percentage of surface markers normalized to total captured EVs was used, which displayed that mDEVs possessed slightly higher expression of MHC-I, MHC-II, and CD86 than that from imDEVs (Figure S9). The observation is consistent with the literature report that mDEVs possess stronger elicitation of immune responses (Yin et al., 2013). We

did not observe significant differences of these marker expressions between light promoted DEVs and native DEVs from both mDCs and imDCs. Taken together, light-induced EV production causes little or no influences on their immune marker expressions. Retaining essential immune surface markers on DEVs is crucial in immunity regulation. The light-promoted DEVs retain immune-modulation functional markers, while having a significantly boosted production rate, which is essential for developing population-based doses at the large scale.

Because the coexpression of MHC-I or MHC-II with CD86 could represent the potency for T cell activation, we analysed such coexpression levels of MHC-I, MHC-II and CD86 in various combinations by utilizing NanoVeiw colocalization imaging. The coexpression of CD63/MHC-I/CD86, CD63/MHC-II/CD86, MHC-I/CD86, MHC-II/CD86, or CD63/CD86 did not show significant changes under different DEV conditions with or without light treatment, although MHC-I or MHC-II alone exhibited a slight reduction after light treatment (Figure 4e and f). Overall, the immune profile patterns are comparable within imDEVs or mDEVs, regardless of light treatment. The mDEVs always possess higher expression of MHC and CD86 markers than that from imDEVs, which is consistent with literature reported observations (Pang et al., 2019; Yin et al., 2013).

3.3 | Light promoted DEVs are internalized the same as the native DEVs

Due to the significance of surface properties and receptors in controlling the EV internalization process (Mulcahy et al., 2014), studying the cellular internalization of light promoted DEVs can precisely evaluate the integral quality and immunological viability for use as a well-controlled therapeutic platform. Currently, the most recognized cellular internalization pathways for EVs are receptor- and raft-mediated endocytosis, phagocytosis, micropinocytosis, and membrane fusion (Feng et al., 2010; Franzen et al., 2014; Gonda et al., 2019; Mckelvey et al., 2015). Here we investigated the cellular internalization of light promoted DEVs using both immune cells (immature JAWS II and IC-21 macrophages) and nonimmune cells (HUVEC cells), compared with native DEVs as the control group (Figure 5). For the early stage of uptake at 1 h, all DEVs were internalized by the three types of cells regardless of the producing DC cell conditions or light treatment conditions (Figure 4a–c). By tracking the lysosomes, the most internalized DEVs were in early endosomes and a few were partially colocalized within the lysosomes. We suspect that the internalization of DEVs could occur through multiple routes including endocytosis, phagocytosis, and membrane fusion (He et al., 2019; Tian et al., 2013). In order to quantitatively evaluate the light-promoted DEVs in terms of their internalization behaviour compared to native DEVs, we used scatterplot analysis to assess the dispersion degree between red fluorescence tracking lysosomes and green fluorescence tracking DEVs. After internalization by immature JAWS II cells, both UV-imDEVs and UV-mDEVs exhibited the same dispersion degree as their control imDEV and mDEVs groups, respectively (Figure 4d). Similarly, we did not observe noticeable differences between light-promoted DEVs and native DEVs for internalization by IC-21 macrophages and HUVEC cells (Figure 4d). Overall, these results validated that the internalization of light-promoted DEVs by either immune cells or nonimmune cells are comparable to native DEVs, which indicates the high integral quality and immunological viability of light-promoted DEVs.

3.4 | Light promoted DEVs are highly biocompatible and immune functional

To evaluate the biocompatibility of light promoted DEVs, we conducted a MTT assay to assess cellular viability after incubation with DEVs from different production conditions. By titrating EV dosages ranging from 1.25×10^8 to 1×10^9 for 24, 48, or 72 h incubation, all imDCs showed excellent viability larger than 90%, regardless of incubation with light promoted DEVs or native DEVs (Figure 6a), which was not affected by incubation time as we tested after 24 and 48 h (Figure S10). More interestingly, light promoted DEVs either from mature or immature conditions led to slightly higher cell viability across all dose ranges, indicating light-promoted DEVs possessed good biocompatibility to potentially be employed in the in vivo study.

To investigate the cellular uptake kinetics and behaviour of light-promoted DEVs, we used confocal imaging to monitor the uptake of DEVs labelled with PKH-26, at time intervals of 1, 2, and 4 h. For the first 4 h, shown in Figure 6(b), the example confocal images for internalizing UV-imDEVs and UV-mDEVs by imDCs exhibited similar increasing rates as their corresponding control groups without light treatment (imDEVs and mDEVs) (quantitative analysis shown in Figure S11). However, after 4 h incubation, till 24 h, we noticed decreased uptake of UV-imDEVs, as well as mDEVs and UV-mDEVs, compared to imDEVs (Figure 6c). Note that UV-imDEVs gave similar reduced uptake after 4 h as the mDEVs regardless of the light treatment conditions (Figure 6c). It has been reported that EVs are more preferentially internalized by their origin parent cells (Jurgielewicz et al., 2020). Thus, native imDEVs were more preferentially internalized by their parent imDCs compared with mDEVs or light promoted DEVs. Additionally, EVs have been shown to either break down or release out around 24 h internalization. Therefore, longer incubation times may not accurately reflect the EV internalization (Jurgielewicz et al., 2020), due to increased breakdown rate. In order to further validate our observation, we used IC-21 macrophage cells to uptake the same EV samples and observed similar uptake trends up to 24 h (Figure 6d). It is worth mentioning that the overall uptake from IC-21 macrophage cells is much slower than imDCs, but has a significant ~ 3-fold higher uptake amount at 24 h. This trend seems to follow the reported

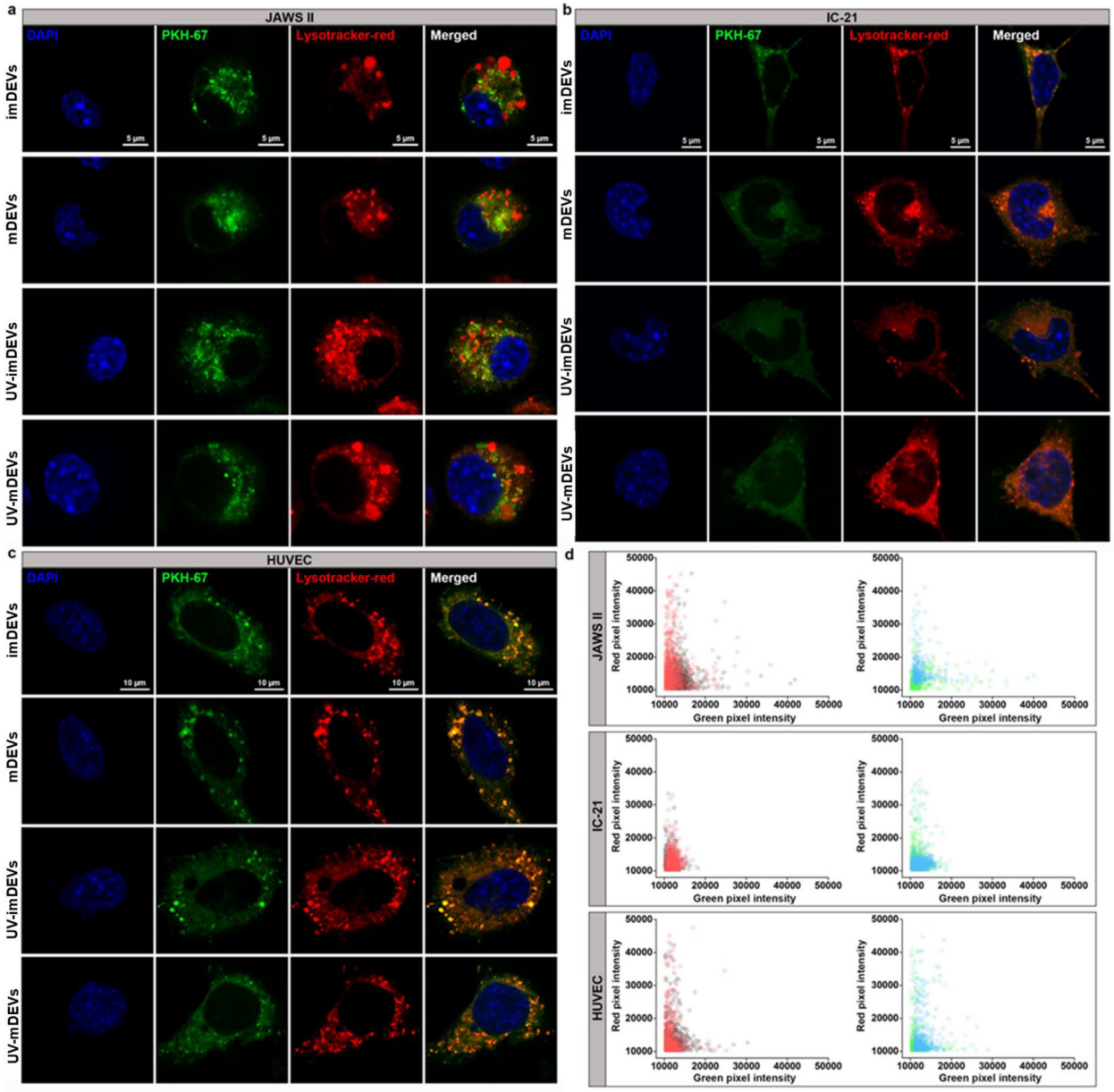

FIGURE 5 Evaluation of the internalization behaviour of UV-promoted DEVs. Confocal images showing the internalization of different DEVs by immature JAWS II cells (a), IC-21 macrophage cells (b), and HUVEC cells (c). DEVs were labelled with PKH-67 in green for incubation of 1 h. Cells were labelled with lysosomal tracker in red and nucleus in blue. (d) Scatter plot analysis of dispersion degree between DEVs internalization and lysosome colocalization. The comparison was made for assessing uptake of UV-imDEVs (red dots) and imDEVs (black dots), as well as UV-mDEVs (blue dots) and mDEVs (green dots) by immature JAWS II cells, IC-21 macrophages, and HUVEC cells

observation that slower first-order rate constant of EV uptake is correlated with higher total cellular uptake amount (Jurgielewicz et al., 2020).

In order to further assess the immunomodulatory function from light-promoted DEVs in eliciting cellular level response, we used flow cytometry to investigate several important immune surface marker expressions (CD11c, MHC-I, MHC-II, CD86) from imDCs after uptaking EVs for 24, 48, and 72 h. We noticed that after 72 h uptake of either UV-mDEVs or mDEVs, imDCs could be significantly elicited to express much higher immune functional markers (Figure 7a-f, Figure S12-S14), indicating the stronger ability of both UV-mDEVs and mDEVs to stimulate in vitro cellular DC maturation. We did not observe noticeable differences from light promoted DEVs compared to native EVs, in terms of the ability for in vitro cellular level immunomodulation (Figure 7d-f). We also monitored the cellular secretion of TNF-α from imDCs after uptaking different EV samples, which essentially indicates DC immune activity. At 72 h uptake, we observed both UV-mDEVs and mDEVs can significantly elicit TNF-α secretion from imDCs, with a ~1.5-fold increase compared to the group of imDEVs and a ~3-fold increase compared to

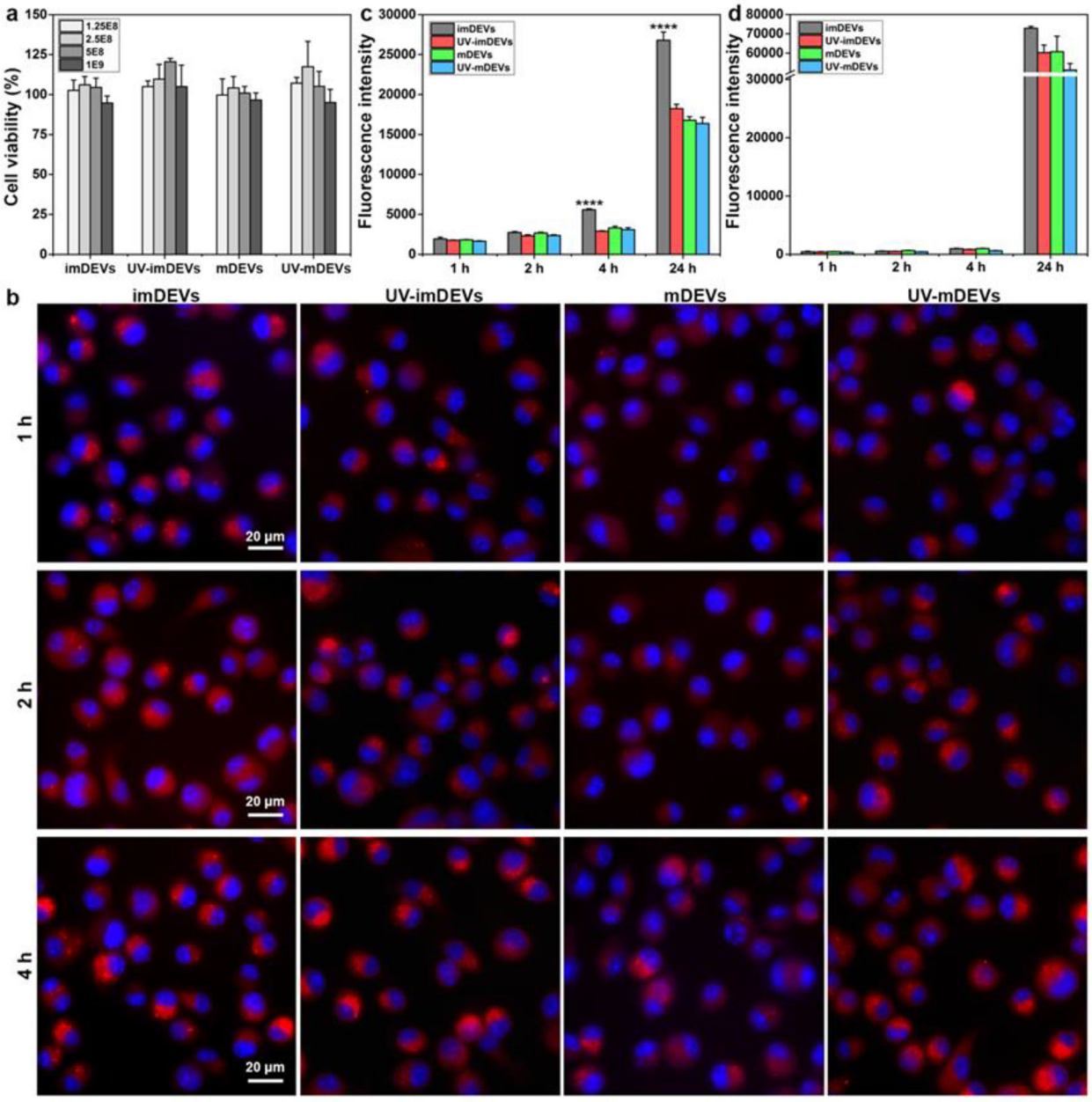

FIGURE 6 In vitro evaluation of biocompatibility and cellular uptake behaviour of light-promoted DEVs. (a) Cell viability analysis of imDCs incubated with light-promoted and native DEVs with dose titrations for 72 h ($n = 5$). (b) Confocal imaging of cellular uptake of light-promoted DEVs compared with native DEVs along time intervals between 1–4 h, using imDCs. (c) Flow cytometry analysis of imDCs for internalizing light-promoted DEVs compared with native DEVs along time intervals between 1–24 h ($n = 3$). (d) Flow cytometry analysis of IC-21 macrophage cells for internalizing light-promoted DEVs compared with native DEVs along time intervals between 1–24 h ($n = 3$). All values are presented as means ± SD. ****$p < 0.0001$

the group of untreated DCs, indicating the higher immunomodulation potential of mDEVs compared to imDEVs (Figure 7g-i), which is consistent with previous reports (Quah & O'Neill, 2005), regardless of light treatment conditions. Moreover, there was no noticeable difference between mDEVs and UV-mDEVs, suggesting the light-promoted DEVs did not exhibit alterations in their intrinsic immunological function compared to native DEVs. Additionally, flow cytometry analysis also validated that cellular immune marker expression ($CD11c^+CD86^+$) increased in a dose-dependent manner through incubation with UV-mDEVs (Figure S15), indicating the direct correlation of cellular immune response with EV uptake.

3.5 | Light promoted DEVs exhibit native in vivo biodistribution and immunogenicity

For safe and successful therapeutic development and clinical applications, understanding the light-promoted DEV in vivo biodistribution profile, immunogenicity, and administration are critical. Therefore, we labelled different DEV samples with a

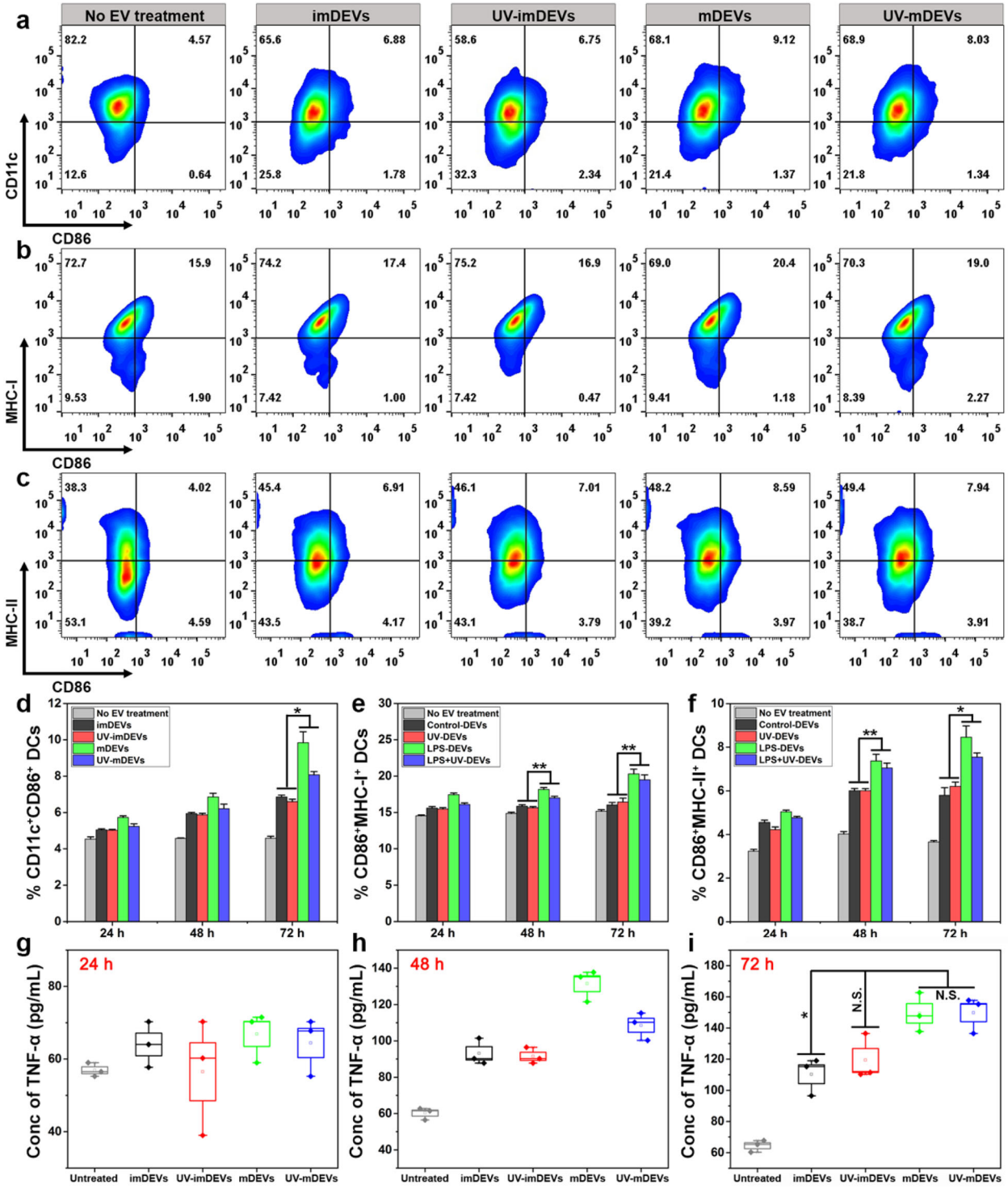

FIGURE 7 Assessment of in vitro immunomodulatory function from light-promoted DEVs. Representative flow cytometry analysis of imDCs incubated with DEVs produced from different conditions. The EV dose is 1×10^9 for 72 h. The imDCs were immunostained with CD11c and CD86 (a), MHC-I and CD86 (b), and MHC-II and CD86 (c). (d-f) Quantitative analysis of immune marker expression level from imDCs after incubation with different DEV samples for 24, 48, and 72 h ($n = 3$), in terms of coexpression of $CD11c^+CD86^+$ (d), $CD86^+MHC\text{-}I^+$ (e), and $CD86^+MHC\text{-}II^+$ (f). (g-i) Quantitative analysis of cellular cytokine TNF-α secretion by imDCs after incubation with different DEV samples for 24 h (g), 48 h (h), and 72 h (i) ($n = 3$). All values are presented as means ± SD. *$p < 0.0332$ and **$p < 0.0021$

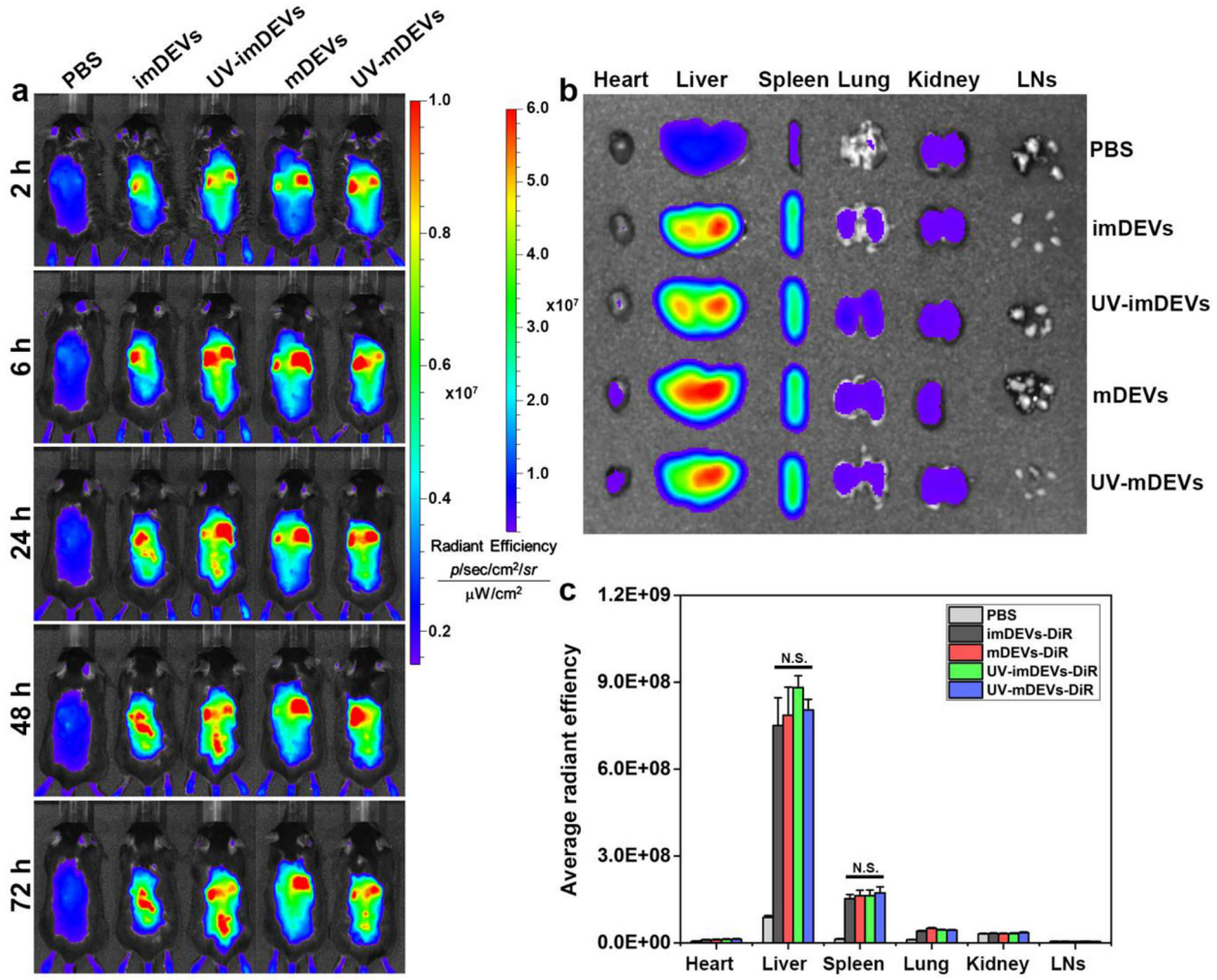

FIGURE 8 In vivo biodistribution analysis of light-promoted DEVs. (a) Representative living in vivo imaging of male C57BL6 mice at different time intervals after intravenous injection of DiR-labelled DEV samples. (b) Ex vivo imaging of major organs harvested from healthy male mice sacrificed at 72 h post injection. (c) The average radiant efficiency ($n = 3$) of different DiR-labelled DEV samples distributed in different organs from figure (b)

near-infrared dye (DiR) and further evaluated their in vivo biodistribution in healthy male and female C57BL6 mice, respectively. Compared to the mice treated with PBS only, DEV treated mice groups showed much higher fluorescent signal 2 h postinjection (Figure 8a). The fluorescent signals were mainly centred in the regions of the liver and gradually spread out along time, followed by a slight decrease at 72 h. To quantitively monitor the fluorescence distribution among organs, we harvested the major organs (heart, liver, spleen, lung, kidney and lymph nodes) from mice post 72 h injection and performed ex vivo imaging (Figure 8b and c). The results consistently showed strong distribution centred mainly in the liver and spleen, over the heart, lung, kidney and lymph nodes, regardless of treatment with light-promoted DEVs or native DEVs. The EVs either from immature DCs or mature DCs did not exhibit any differences neither. To investigate whether the gender of mouse affects the biodistribution profile of these DEVs, we further performed the in vivo and ex vivo imaging parallelly using healthy female C57BL6 mice. As expected, the displayed biodistribution profile was consistent with that from male mice (Figure S16). Overall results support that light-promoted DEVs possess consistent in vivo biodistribution profiles as the naturally derived DEVs, and they are well tolerated and can be safely administrated without concerns.

As primary peripheral lymphoid organs, the spleen and LNs play an important role in governing the immune response against foreign substances. Therefore, we further investigated the in vivo immunogenicity of these DEVs by monitoring immune marker expression from spleen and LNs derived total splenocytes and lymphocytes at 72h post injection, using flow cytometry analysis. The expression levels of $CD11c^+CD86^+$(Figure 9a), $MHC\text{-}I^+CD86^+$(Figure 9b), $MHC\text{-}II^+CD86^+$(Figure 9c) in total splenocytes between native and light-promoted DEV groups did not show noticeable differences. Meanwhile, both mature and immature DEV groups also exhibited similar immune marker expressions from both total splenocytes (Figure 9d) and lymphocytes (Figure 9e, Figure S17), which is comparable to the PBS treated negative control group. The corresponding gating strategy for

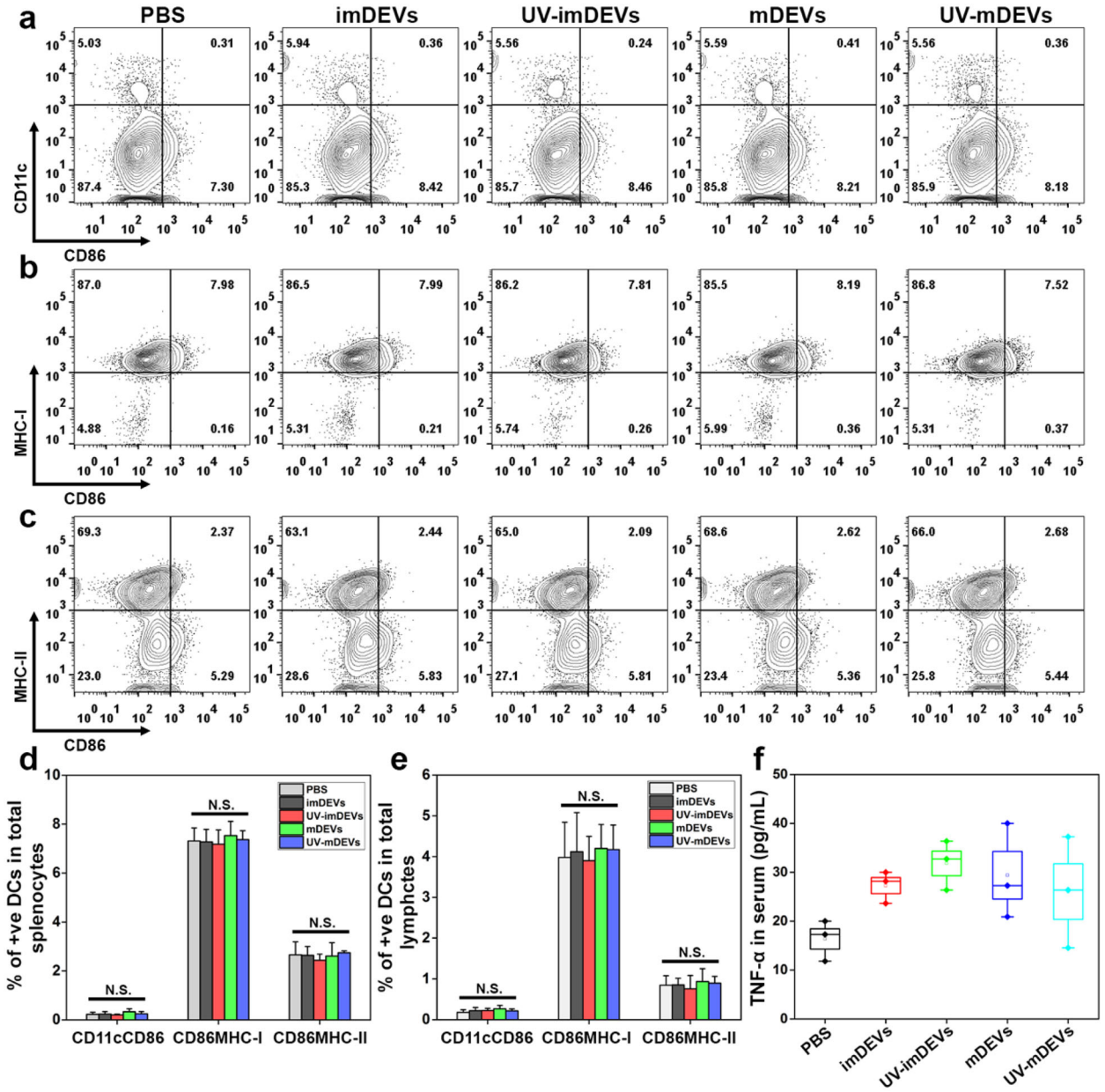

FIGURE 9 In vivo evaluation of immunogenicity of light-promoted DEVs. Representative flow cytometry analysis of $CD11c^+CD86^+$ (a), MHC-I^+CD86^+ (b), and MHC-II^+CD86^+ (c) in total splenocytes from healthy male mice treated with different DEV samples at 72 h post injection ($n = 3$). PBS injection was set as the negative control. Quantitative analysis of the expression level of immune markers from total splenocytes (d) and LNs (e) ($n = 3$). (f) Cytokine level of TNF-α in serum from healthy male mice at 72 h post injection with different DEV samples. PBS injection was set as the negative control ($n = 3$)

flow cytometry analysis of splenocytes and lymphocytes was provided in Supporting Information (Figure S18). The result strongly supports that light-promoted DEVs are well tolerated with no immunogenic concerns and are well suited to serve as natural drug delivery carriers. We further tested TNF-α secretion levels in the serum 72 h post mice intravenous injection, which showed a slight increase after treatment with these DEV samples compared to the negative control group treated with PBS only. Such slight elicitation on TNF-α secretion may be due to the import of TNF-α intrinsically carried by DEVs (Figure 9f). Although the in vitro cellular level study showed significant differences in TNF- α secretion between imDEVs and mDEVs, the in vivo system is more tolerant and may not be as straightforward as in vitro system. Collectively, we validated that light-promoted DEVs possess as little or no immunogenicity as their native DEVs, which is beneficial for serving as drug delivery carriers and development into therapeutic agents. The light-promoted DEVs exhibit excellent tolerance like the native DEVs without safety concerns while having more than 13-fold higher production rate.

4 | CONCLUSION

The use of EVs as alternative drug delivery systems has gained tremendous interest, due to their intrinsic properties, such as natural cellular origin, good biocompatibility and safety, stable and long circulation time in the human body, versatile regulatory functions, and excellent targeting ability (Elliott & He, 2021; Liang et al., 2021). However, due to the limited cellular production rate, harvesting good quality EVs at the necessary scale is always a bottleneck challenge for clinical translation. Our study explores a new opportunity using light stimulation for parent DCs to produce immune functional DEVs with more than 13-fold enhancement in production rate, while remaining good integral quality, biocompatibility, cellular internalization ability, and immunogenicity. Under our optimized light treatment condition, the method is very simple, straightforward, low cost, and generic for promoting other cell types. The protocol can be easily adapted into cell culture incubators or bioreactors on demand at the manufacturing scale, without the requirement of specific equipment setup. We conducted a series of quality validation of light-promoted DEVs, in terms of size, zeta potential, morphology, immune surface markers and cytokines, biocompatibility, ROS production, cellular uptake behaviour, and immune-modulation ability on eliciting cellular responses, as well as their cellular internalization behaviour. We also validated the biodistribution, immunogenicity, and administration safety using light-promoted DEVs in mice models from both male and female genders. Taken together, the data supports that light promoted DEVs are in excellent quality, high biocompatibility, and immune functional for serving as a ideal therapeutic platform with scalable production.

Despite EV-based therapeutic and diagnostic applications having been intensively explored, the in-depth understanding of DEVs and their immune functions during the production process with light induction has not been investigated elsewhere. Our study provides the necessary quantitative information for evaluating light promoted DEVs, corelating their immune surface marker expressions (MHC-I, MHC-II, CD86), cytokine deposit (TNF-α), and EV generic surface marker expressions (CD63, CD9, CD81) with cellular production parameters, which could build good evidence for further therapeutic development. The coexpression levels of those markers measured by NanoView analysis also provide precision immune profiles on light-promoted DEVs for quantitative therapeutic assessment. The in vivo biodistribution and immunogenicity study also demonstrated no significant differences between light-promoted DEVs and native DEVs, which proves the strong feasibility for using optimized light induction for promoting high-rate production of DEVs in therapeutic development.

It has been reported that UVB irradiation (280–315 nm) could elevate cellular oxidative pressure and secret EVs for communicating protective messages during oxidative stress (Liu et al., 2019; Shen et al., 2020). Our light induction wavelength is far from UVB at 365 nm. We observed that 365 nm light treatment at the level of low dose we employed does not increase ROS production for activating the cellular oxidative stress pathway, although the cause for such light induced high-rate production of EVs is not certain. We will conduct more investigation in the future to continually understand the mechanism. Presently, both our observation and other reported studies (Wong et al., 2015) indicated that longer wavelength at 365 nm light does not impair cell growth or affect gene expression. Under our optimized light condition (0.096 W/cm^2 for 30 min), cells are enabled to produce good quality EVs in high speed. Using extreme light exposure time and intensity, such as 0.16 W/cm^2 which we investigated in Figure S5, may have a negative impact on cell growth. We observed that over irradiated cells are still be able to recover and reach90–100% confluency in 6 days for passaging and subculture.

The current study was mainly focused on the intrinsic immunoregulatory function of DEVs using light induced high speed production. The produced EVs are readily available for loading with drugs, specific tissue targeting, or immunotherapeutic agents, to develop EV-based therapies, drug delivery, and vaccines. More opportunities including surface engineering and modification could also be developed down the road by utilizing the existence of specific molecules on EV surfaces, such as MHC molecules, tetraspanins family, or integrin family, to target specific recipient cells and mediate cargo transfer and cellular responses. We foresee this simple method could bring a new solution for developing EV-based therapeutics at a large scale.

ACKNOWLEDGEMENTS

The authors would like to thank Interdisciplinary Center for Biotechnology Research (ICBR) core facility at the University of Florida. The authors would also like to thank Dr. Cory Berkland at the University of Kansas for providing JAWS II cell line from ATCC. This project is supported by NIH NIGMS MIRA award 1R35GM133794 and USDA-NIFA 2017-67021-26600 to Dr. Mei He with corresponding contact: mhe@cop.ufl.edu.

CONFLICTS OF INTEREST

The authors declare no conflict of interest.

ORCID

Mei He https://orcid.org/0000-0001-5316-9326

REFERENCES

Chaput, N. (2006). Dendritic cell derived-exosomes: Biology and clinical implementations. *Journal of Leukocyte Biology*, *80*(3), 471–478.
Elliott, R. O., & He, M. (2021). Unlocking the power of exosomes for crossing biological barriers in drug delivery. *Pharmaceutics*, *13*(1), 122.

Feng, Du, Zhao, W.-L., Ye, Y.-Y., Bai, X.-C., Liu, R.-Q., Chang, L-Fu, Zhou, Q., & Sui, S.-F. (2010). Cellular internalization of exosomes occurs through phagocytosis. *Traffic (Copenhagen, Denmark)*, *11*(5), 675–687.

Fernández-Delgado, I., Calzada-Fraile, D., & Sánchez-Madrid, F. (2020). Immune regulation by dendritic cell extracellular vesicles in cancer immunotherapy and vaccines. *Cancers (Basel)*, *12*(12), 3558.

Franzen, C. A., Simms, P. E., Van Huis, A. F., Foreman, K. E., Kuo, P. C., & Gupta, G. N. (2014). Characterization of uptake and internalization of exosomes by bladder cancer cells. *BioMed Research International*, *2014*, 619829.

Gao, Li, Yuan, T., Zhou, C., Cheng, P., Bai, Q., Ao, J., Wang, W., & Zhang, H. (2013). Effects of four commonly used UV filters on the growth, cell viability and oxidative stress responses of the Tetrahymena thermophila. *Chemosphere*, *93*(10), 2507–2513.

Gary, A.-S., & Rochette, P. J. (2020). Apoptosis, the only cell death pathway that can be measured in human diploid dermal fibroblasts following lethal UVB irradiation. *Science Reports*, *10*(1), 18946.

Ghossoub, R., Chéry, M., Audebert, S., Leblanc, R., Egea-Jimenez, A. L., Lembo, F., Mammar, S., Le Dez, F., Camoin, L., Borg, J.-P., Rubinstein, E., David, G., & Zimmermann, P. (2020). Tetraspanin-6 negatively regulates exosome production. *PNAS*, *117*(11), 5913–5922.

Gonda A., Kabagwira J., Senthil G N., Wall N R., Internalization of exosomes through receptor-mediated endocytosis. *Molecular Cancer Research*, *17*(2) (2019) 337–347.

Gurunathan, S., Kang, M.-H., Jeyaraj, M., Qasim, M., & Kim, J.-H. (2019). Review of the Isolation, Characterization, Biological Function, and Multifarious Therapeutic Approaches of Exosomes. *Cells*, *8*(4), 307.

He, F., Ye, Ze-Yu, Zhao, Li-D., Yin, B.-C., & Ye, B-Ce (2019). Probing exosome internalization pathways through confocal microscopy imaging. *Chemical Communications (Cambridge, England)*, *55*(93), 14015–14018.

Jafari, D., Malih, S., Eini, M., Jafari, R., Gholipourmalekabadi, M., Sadeghizadeh, M., & Samadikuchaksaraei, A. (2020). Improvement, scaling-up, and downstream analysis of exosome production. *Critical Reviews in Biotechnology*, 1098–1112.

Jurgielewicz, B. J., Yao, Y., & Stice, S. L. (2020). Kinetics and specificity of HEK293T extracellular vesicle uptake using imaging flow cytometry. *Nanoscale Research Letters*, *15*(1), 170.

Lamichhane, T. N., & Jay, S. M. (2018). Production of extracellular vesicles loaded with therapeutic cargo. *Methods in Molecular Biology*, *1831*, 37–47.

Lázaro-Ibáñez, E., Sanz-Garcia, A., Visakorpi, T., Escobedo-Lucea, C., Siljander, P., Ayuso-Sacido, Á., & Yliperttula, M. (2014). Different gDNA content in the subpopulations of prostate cancer extracellular vesicles: Apoptotic bodies, microvesicles, and exosomes. *Prostate*, *74*(14), 1379–1390.

Li, P., Kaslan, M., Lee, S. H., Yao, J., & Gao, Z. (2017). Progress in exosome isolation techniques. *Theranostics*, *7*(3), 789–804.

Liang, Y., Duan, Li, Lu, J., & Xia, J. (2021). Engineering exosomes for targeted drug delivery. *Theranostics*, *11*(7), 3183–3195.

Liu, J., Zhu, H., Premnauth, G., Earnest, K. G., Hahn, P., Gray, G., Queenan, J. A., Prevette, L. E., Abdulsalam, S. F., Kadekaro, A. L., & Merino, E. J. (2019). UV cell stress induces oxidative cyclization of a protective reagent for DNA damage reduction in skin explants. *Free Radical Biology and Medicine*, *134* 133–138.

Markov, O., Oshchepkova, A., & Mironova, N. (2019). Immunotherapy Based on Dendritic Cell-Targeted/-Derived Extracellular Vesicles-A Novel Strategy for Enhancement of the Anti-tumor Immune Response. *Frontiers in Pharmacology*, *10*, 1152.

Masuma, R., Kashima, S., Kurasaki, M., & Okuno, T. (2013). Effects of UV wavelength on cell damages caused by UV irradiation in PC12 cells. *Journal of Photochemistry and Photobiology B Biology*, *125* 202–208.

Mckelvey, K. J., Powell, K. L., Ashton, A. W., Morris, J. M., & Mccracken, S. A. (2015). Exosomes: Mechanisms of uptake. *Journal of Circulating Biomarkers*, *4*, 7.

Mcneill, B., Ostojic, A., Rayner, K. J., Ruel, M., & Suuronen, E. J. (2019). Collagen biomaterial stimulates the production of extracellular vesicles containing microRNA-21 and enhances the proangiogenic function of CD34(+) cells. *Faseb Journal*, *33*(3), 4166–4177.

Mitchell, J. P., Court, J., Mason, M. D., Tabi, Z., & Clayton, A. (2008). Increased exosome production from tumour cell cultures using the Integra CELLine Culture System. *Journal of Immunological Methods*, *335*(1-2), 98–105.

Morelli, A. E., Larregina, A. T., Shufesky, W. J., Sullivan, M. L. G., Stolz, D. B., Papworth, G. D., Zahorchak, A. F., Logar, A. J., Wang, Z., Watkins, S. C., Falo, L. D., & Thomson, A. W. (2004). Endocytosis, intracellular sorting, and processing of exosomes by dendritic cells. *Blood*, *104*(10), 3257–3266.

Mulcahy, L. A., Pink, R. C., & Carter, D. R. F. (2014). Routes and mechanisms of extracellular vesicle uptake. *Journal of Extracellular Vesicles*, *3*, 24641.

Munich S., Sobo-Vujanovic A., Buchser W J., Beer-Stolz D., & Vujanovic N. L. (2012). Dendritic cell exosomes directly kill tumor cells and activate natural killer cells via TNF superfamily ligands. *Oncoimmunology*, *1*(7), 1074–1083.

Ogasawara, M., Miyashita, M., Yamagishi, Y., & Ota, S. (2020). Immunotherapy employing dendritic cell vaccination for patients with advanced or relapsed esophageal cancer. *Therapeutic Apheresis and Dialysis: Official Peer-Reviewed Journal of the International Society for Apheresis, the Japanese Society for Apheresis, the Japanese Society for Dialysis Therapy*, *24*(5), 482–491.

Pang, X.-L., Wang, Z.-G., Liu, L., Feng, Y.-H., Wang, J.-X., Xie, H.-C., Yang, X.-L., Li, J.-F., & Feng, G.-W. (2019). Immature dendritic cells derived exosomes promotes immune tolerance by regulating T cell differentiation in renal transplantation. *Aging (Albany NY)*, *11*(20), 8911–8924.

Perez, C. R., & De Palma, M. (2019). Engineering dendritic cell vaccines to improve cancer immunotherapy. *Nature Communication*, *10*(1), 5408.

Piffoux, M., Nicolás-Boluda, A., Mulens-Arias, V., Richard, S., Rahmi, G., Gazeau, F., Wilhelm, C., & Silva, A. K.A. (2019). Extracellular vesicles for personalized medicine: The input of physically triggered production, loading and theranostic properties. *Advanced Drug Delivery Reviews*, *138*, 247–258.

Pitt, J. M., André, F., Amigorena, S., Soria, J.-C., Eggermont, A., Kroemer, G., & Zitvogel, L. (2016). Dendritic cell-derived exosomes for cancer therapy. *Journal of Clinical Investigation*, *126*(4), 1224–1232.

Pitt, J. M., Charrier, M., Viaud, S., André, F., Besse, B., Chaput, N., & Zitvogel, L. (2014). Dendritic cell-derived exosomes as immunotherapies in the fight against cancer. *Journal of Immunology*, *193*(3), 1006–1011.

Quah, B. J.C., & O'neill, H. C. (2005). The immunogenicity of dendritic cell-derived exosomes. *Blood Cells, Molecules & Diseases*, *35*(2), 94–110.

Riquelme, J. A., Takov, K., Santiago-Fernández, C., Rossello, X., Lavandero, S., Yellon, D. M., & Davidson, S. M. (2020). Increased production of functional small extracellular vesicles in senescent endothelial cells. *Journal of Cellular and Molecular Medicine*, *24*(8), 4871–4876.

Robbins, P. D., & Morelli, A. E. (2014). Regulation of immune responses by extracellular vesicles. *Nature Reviews Immunology*, *14*(3), 195–208.

Sadeghzadeh, M., Bornehdeli, S., Mohahammadrezakhani, H., Abolghasemi, M., Poursaei, E., Asadi, M., Zafari, V., Aghebati-Maleki, L., & Shanehbandi, D. (2020). Dendritic cell therapy in cancer treatment; the state-of-the-art. *Life Sciences*, *254*, 117580.

Saxena, M., Balan, S., Roudko, V., & Bhardwaj, N. (2018). Towards superior dendritic-cell vaccines for cancer therapy. *Nature Biomedical Engineering*, *2*(6), 341–346.

Shen, Z., Sun, J., Shao, J., & Xu, J. (2020). Ultraviolet B irradiation enhances the secretion of exosomes by human primary melanocytes and changes their exosomal miRNA profile. *Plos One*, *15*(8), e0237023.

Surman, M., Drożdż, A., Stępień, E., & Przybyło, M. (2019). Extracellular vesicles as drug delivery systems - Methods of production and potential therapeutic applications. *Current Pharmaceutical Design*, *25*(2), 132–154.

Thery, C., Amigorena, S., Raposo, G., & Clayton, A. (2006). Isolation and characterization of exosomes from cell culture supernatants and biological fluids. *Current Protocols in Cell Biology*, *3*.

Théry, C., Witwer, K. W., Aikawa, E., Alcaraz, M. J., Anderson, J. D., Andriantsitohaina, R., Antoniou, A., Arab, T., Archer, F., Atkin-Smith, G. K., Ayre, D. C., Bach, J.-M., Bachurski, D., Baharvand, H., Balaj, L., Baldacchino, S., Bauer, N. N., Baxter, A. A., Bebawy, M., … Zuba-Surma, E. K. (2018). Minimal information for studies of extracellular vesicles 2018 (MISEV2018): A position statement of the International Society for Extracellular Vesicles and update of the MISEV2014 guidelines. *Journal of Extracellular Vesicles*, *7*(1), 1535750.

Tian, H., & Li, W. (2017). Dendritic cell-derived exosomes for cancer immunotherapy: Hope and challenges. *Annals of Translational Medicine*, *5*(10), 221.

Tian, T., Zhu, Y.-L., Hu, F-Hu, Wang, Y.-Y., Huang, N.-P., & Xiao, Z.-D. (2013). Dynamics of exosome internalization and trafficking. *Journal of Cellular Physiology*, *228*(7), 1487–1495.

Utsugi-Kobukai, S., Fujimaki, H., Hotta, C., Nakazawa, M., & Minami, M. (2003). MHC class I-mediated exogenous antigen presentation by exosomes secreted from immature and mature bone marrow derived dendritic cells. *Immunology Letters*, *89*(2-3), 125–131.

Wang, Y., Xiang, Y., Xin, V. W., Wang, X.-W., Peng, X.-C., Liu, X.-Q., Wang, D., Li, N., Cheng, J.-T., Lyv, Y.-N., Cui, S.-Z., Ma, Z., Zhang, Q., & Xin, H.-W. (2020). Dendritic cell biology and its role in tumor immunotherapy. *Journal of Hematology & Oncology*, *13*(1), 107.

Wong, D. Y., Ranganath, T., & Kasko, A. M. (2015). Low-dose, long-wave uv light does not affect gene expression of human mesenchymal stem cells. *Plos One*, *10*(9), e0139307.

Yamashita, T., Takahashi, Y., & Takakura, Y. (2018). Possibility of exosome-based therapeutics and challenges in production of exosomes eligible for therapeutic application. *Biological & Pharmaceutical Bulletin*, *41*(6), 835–842.

Yang, X., Chen, J., Wang, N., Liu, Z., & Li, Y. (2018). Clinical use of dendritic cell-derived exosomes for hepatocellular carcinoma immunotherapy: How far we are?. *Journal of Hepatology*, *69*(4), 984–986.

Yang, Z., Shi, J., Xie, J., Wang, Y., Sun, J., Liu, T., Zhao, Y., Zhao, X., Wang, X., Ma, Y., Malkoc, V., Chiang, C., Deng, W., Chen, Y., Fu, Y., Kwak, K. J., Fan, Y., Kang, C., Yin, C., … Lee, L. J. (2020). Large-scale generation of functional mRNA-encapsulating exosomes via cellular nanoporation. *Nature Biomedical Engineering*, *4*(1), 69–83.

Yin, W., Ouyang, S., Li, Y., Xiao, B., & Yang, H. (2013). Immature dendritic cell-derived exosomes: A promise subcellular vaccine for autoimmunity. *Inflammation*, *36*(1), 232–240.

SUPPORTING INFORMATION

Additional supporting information may be found in the online version of the article at the publisher's website.

How to cite this article: Ruan, S., Erwin, N., & He, M. (2022). Light-induced high-efficient cellular production of immune functional extracellular vesicless. *Journal of Extracellular Vesicles*, *11,* e12194. https://doi.org/10.1002/jev2.12194